Failure of fracture toughness criterion at small scales

Yangyang Cheng,[1] Long Yu,[1] Lirong Chen,[1] Wenbin Liu,[1] Xin Yi,[1,*] and Huiling Duan[1,2,†]

[1]*State Key Laboratory for Turbulence and Complex Systems, Department of Mechanics and Engineering Science, BIC-ESAT, College of Engineering, Peking University, Beijing 100871, People's Republic of China*

[2]*CAPT, HEDPS and IFSA Collaborative Innovation Center of MoE, Peking University, Beijing 100871, People's Republic of China*

(Received 7 April 2019; published 11 November 2019)

Fracture toughness testing at small scales is widely adopted for materials of limited size. Recent experimental results demonstrate that the fracture toughness of single-crystal tungsten decreases by half as the specimen size drops equally from the order of several dozen micrometers to 1 μm. To explore this size-dependent fracture feature, we construct a fracture model by combining the Griffith strength theory and elastic-damage law. It is shown that as the specimen scales down to a critical size, the fracture behavior changes from the fracture toughness domination to the strength domination, leading to a seeming decrease of the fracture toughness. Reviewing mechanical fracture testing of different brittle materials at small scales, we found that their fracture is dominated by fracture strength instead of fracture toughness, which explains why the reported values of fracture toughness obtained from the microscale testing are significantly less than the corresponding ones measured at the macroscale. Our study has profound guiding significance for the characterization of the fracture toughness at small scales.

DOI: 10.1103/PhysRevMaterials.3.113602

I. INTRODUCTION

Fracture toughness is commonly defined by the critical stress intensity factor K_c, which is used to characterize the resistance of materials against crack extension [1–3]. Conventional measurement approaches of K_c via bend specimen or compact specimen configurations require a sufficiently large specimen in which a crack with a sharp tip and well-defined shape can be introduced via cyclic loading [4,5]. However, it is difficult to perform cyclic loading at a characterized specimen size below the centimeter scale, thus hardly characterizing K_c in an appropriate manner based on conventional measurements [6,7].

This problem is mitigated by the fracture toughness testing at small scales with a combination of focused ion beam (FIB) milling and small-scale mechanical testing approaches [8–12]. In the toughness testing, the FIB milling is employed to fabricate a beam of nanoscale or microscale and make a sharp notch of a root radius around tens of nanometers, which can be viewed as a crack [13–16], and then the cracked beam is subjected to a bending test in which the loading force is recorded to calculate the fracture toughness as the crack propagation occurs [17–21] (as detailed in Part 1 of the Supplemental Material (SM) [22]). This method at small scales is universal and not restricted by the material types and geometrical sizes.

It is known that the stress intensity factor K scales with the applied stress and the specimen size (referring to crack length, thickness, and width) [2,4]. Under a specific configuration, the fracture toughness K_c as an intrinsic property of brittle materials reveals a special relationship between the fracture stress and the crack length: The smaller the crack length, the larger the fracture stress at which the crack propagates, and vice versa [23,24]. On this basis, from the macroscale testing of K_c to the microscale, the fracture stress would increase around 30-fold due to the size variation from around dozens of millimeters to around several micrometers, and probably exceed the fracture strength. It is desirable to determine the validity of K_c in dominating the fracture behavior at small scales.

Recent experimental studies about the effect of specimen size on the fracture toughness of the crack system $\{100\}\langle 100\rangle$ of single-crystal tungsten indicate that as the tungsten specimen scales down from several dozens of micrometers to less than 1 μm, the fracture toughness obtained decreases by half [18]. Moreover, there exists an inflection point at the crack length about 2 μm, above which the fracture toughness varies very little and is close to the value from the macroscale testing, yet below which it drops dramatically [18]. Since the geometries of different specimens in Ref. [18] are similar, the size dependence of the fracture toughness shall not result from the variation of specimen thickness, i.e., the stress-state transition (plane stress or plane strain) [25–27]. Here we develop a theoretical model to understand the underlying mechanism of size-dependent fracture toughness. It is shown that with the downscaling of specimen size, the fracture toughness-controlled fracture changes to strength-controlled fracture, which leads to the seeming decrease of the fracture toughness. Because the geometries of the specimens are similar, it is reasonable to select the variation of crack length to represent the change of specimen size. On this basis, the critical crack length distinguishing the fracture mode can be expressed quantitatively by our model. Our results shed light on the validity of the fracture toughness testing at small scales.

*Corresponding author: xyi@pku.edu.cn
†Corresponding author: hlduan@pku.edu.cn

TABLE I. Summary of crack length $a(\mu\text{m})$, width $W(\mu\text{m})$, ligament length $(W-a)(\mu\text{m})$, thickness $B(\mu\text{m})$ and loading span $L(\mu\text{m})$, crack-geometry factor ψ, ratio $\alpha=(W-a)^2/W^2$, and fracture toughness $K_{\text{Q}}(\text{MPa m}^{1/2})$ for tungsten specimens with different sizes [18].

a	W	$(W-a)$	B	L	ψ	α	K_{Q}
0.2	0.8	0.6	0.5	2.5	1.92	0.56	1.48 ± 0.1
0.5	1.5	1	1	4	2.05	0.44	1.86 ± 0.1
0.7	2.5	1.8	2	6.5	1.96	0.52	2.34 ± 0.1
2.1	5	2.9	4.5	8	2.3	0.34	3.02 ± 0.3
5.5	15	9.5	12	24	2.02	0.35	3.18 ± 0.3
16.5	45	28.5	25.5	72	2.13	0.4	3.43

II. RESULTS AND DISCUSSION

We first explore whether the fracture toughness measured at small scales in Ref. [18] is valid. For the specimen at the macroscale, according to ASTM standard E399-17 [4], the crack length a is specified to be not less than $l_{\text{a}}=2.5(K_{\text{Q}}/\sigma_{\text{y}})^2$ with K_{Q} as the conditional fracture toughness and σ_{y} as the yielding strength of the material. This specification guarantees the applicability of linear-elastic fracture mechanics (LEFM). The standard is constructed based on the three-point bend specimen configuration of $a/W=0.5$ with W as the specimen width, while at small scales the widely used configuration is cantilever specimen. Our finite element simulations (see Part 2 in the SM [22]) reveal that l_{a} depends on the type of specimen configuration and the value of a/W. For the cantilever specimen configuration of $a/W=0.5$, our numerical results indicate that $l_{\text{a}}=1.4(K_{\text{Q}}/\sigma_{\text{y}})^2$, different from that of the three-point bend specimen configuration. a/W in Ref. [18] ranges from 0.25 to 0.42, and l_{a} varies from $0.24(K_{\text{Q}}/\sigma_{\text{y}})^2$ to $0.87(K_{\text{Q}}/\sigma_{\text{y}})^2$ accordingly. The detailed calculation on l_{a} is provided in Part 2 of the SM [22]. In the present paper, for simplicity, as to the cantilever configuration with $a/W<0.3$, $a\geqslant l_{\text{a}}=0.25(K_{\text{Q}}/\sigma_{\text{y}})^2$ is taken, while as to $0.3\leqslant a/W\leqslant 0.45$, $a\geqslant l_{\text{a}}=(K_{\text{Q}}/\sigma_{\text{y}})^2$ is taken. To the best of our knowledge, almost all experimental reports [17,20,28] characterizing the fracture toughness at small scales adopt the standard of ASTM mainly for the three-point bend and compact tension specimen configurations, which is not appropriate for the cantilever specimen configuration.

To ensure the reliability of the testing of K_{Q} in a plane-strain condition, both the specimen thickness B and the difference between the width W and crack length a are required as $B\geqslant 2.5(K_{\text{Q}}/\sigma_{\text{y}})^2$ and $(W-a)\geqslant 2.5(K_{\text{Q}}/\sigma_{\text{y}})^2$ derived from numerous experimental results [3,4,29]. However, actually the effect of $(W-a)$ on the measurement of fracture toughness is limited, and the requirement on it is not as strict as a and B, which is discussed in details in Ref. [29]. For the cantilever specimen configuration considered here, we adopt the same specification for B and W.

Table I presents the geometrical size and fracture toughness of the microcantilever specimen of single-crystalline tungsten in Ref. [18]. It has been reported that under uniaxial compression for ⟨100⟩-oriented tungsten pillars, the yielding strength σ_{y} is around 2.3 GPa at specimen diameters of 0.5 μm, 1 μm, and 2 μm, and around 1.6 GPa at a specimen diameter of 5 μm [14]. Therefore, we take $\sigma_{\text{y}}=2.3$ GPa for the first four specimens with $(W-a)\leqslant 2.9$ μm as listed in Table I and $\sigma_{\text{y}}=1.6$ GPa for the rest specimens of $(W-a)>2.9$ μm.

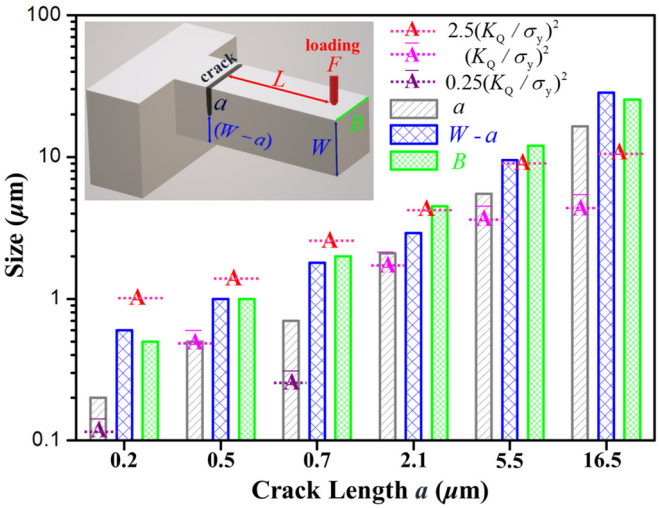

FIG. 1. Comparison between the microcantilever size and the size required by our proposed standard. The inset shows the schematic of the microcantilever with a crack.

For easy visualization, the specimen size [referring to a, $(W-a)$ and B] and the size required by our proposed standard as discussed above are depicted in Fig. 1. It is shown that the crack length a of all six specimens is not less than the required size l_{a}, verifying that LEFM can exactly characterize the stress field ahead of the crack tip. Regarding the thickness B, its value in the small specimens is slightly less than the corresponding required size $2.5(K_{\text{Q}}/\sigma_{\text{y}})^2$. Strictly, this means that the crack tip is not completely situated for plane strain. However, the fractographic observation indicates that the crack plane is almost flat, and there are no pronounced shear lips and crack deflection around the edges [18], which confirms that the deformation around the crack tip is predominately under the plane-strain condition. The above analysis eliminates the possibility that the variation of K_{Q} is resulted from the inapplicability of LEFM and the change of stress state.

Based on the thin beam elasticity theory, the maximum nominal fracture stress σ_{n} in the crack plane is given by

$$\sigma_{\text{n}}=\frac{6FL}{BW^2}, \tag{1}$$

where F is the loading force when the fracture occurs and L is the loading span. Considering that the crack has no load-carrying capacity, the net width of the plane should be $(W-a)$, then the maximum net-section fracture stress σ_{e} ahead of the crack tip is given by

$$\sigma_{\text{e}}=\frac{6FL}{B(W-a)^2}. \tag{2}$$

Although the cantilever specimen configuration in Ref. [18] is not an ideal thin beam, σ_{n} and σ_{e} obtained from the thin beam theory are consistent with our finite element simulation results (listed in Table SII in Part 3 of the SM [22]). For the

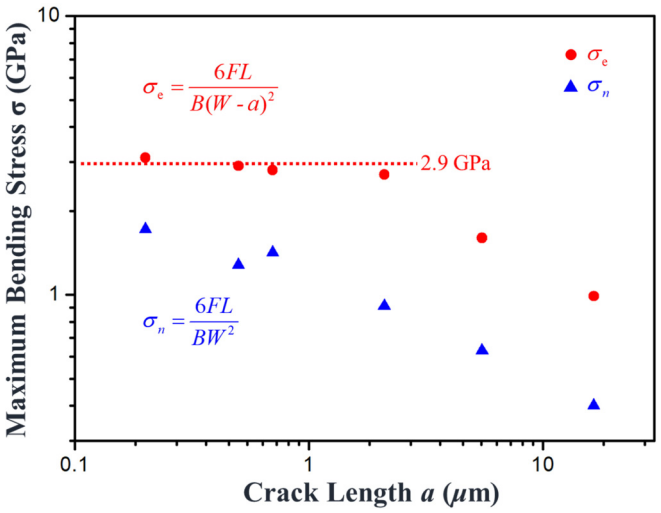

FIG. 2. Maximum bending stress versus crack length for specimens of different sizes.

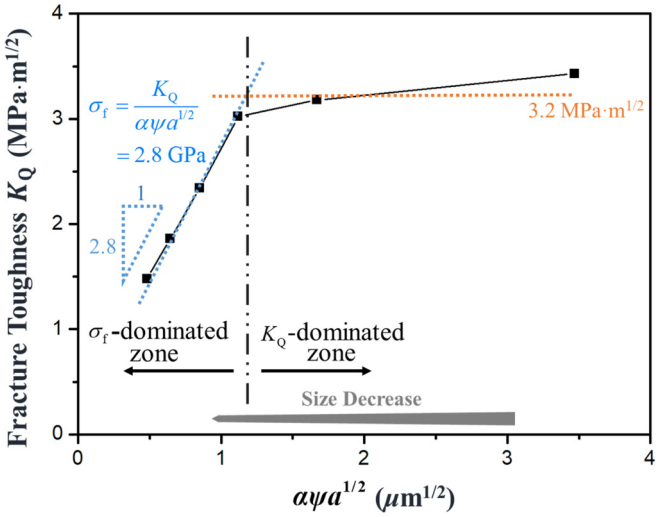

FIG. 3. Fracture toughness K_Q as a function of $\alpha\psi a^{1/2}$ for specimens of different sizes.

small specimens with a of 0.2 μm, 0.5 μm, 0.7 μm, and 2.1 μm, σ_e is insensitive to the crack length a and maintains around 2.9 GPa with a standard deviation of 0.17 (see Fig. 2). In contrast, regarding σ_n, the average value is 1.3 GPa with a standard deviation of 0.33. In this situation, we make a postulate that as the specimen is smaller than a critical size, its fracture is determined by the critical net-section stress, i.e., fracture strength. In other words, there exists a transition from fracture toughness-dominated fracture to fracture strength-dominated fracture with the decrease in the specimen size.

According to LEFM, the stress intensity factor K_I for the mode I crack is

$$K_I = \sigma\psi a^{1/2}, \tag{3}$$

where σ is the remote applied stress far away from the crack plane (equivalent to σ_n for cantilever specimen configuration), a characterizes the crack length (for an internal crack, a is one half of the length; for an edge crack, a is the length), and ψ is crack-geometry factor [2]. If the fracture of the small specimens is controlled by the fracture strength σ_f or equivalently σ_e, the fracture toughness of the small specimens can be given as

$$K_Q = \sigma_f\alpha\psi a^{1/2}, \tag{4}$$

where $\alpha = \sigma_n/\sigma_e$ or equivalently $\alpha = (W-a)^2/W^2$. Eq. (4) indicates that K_Q depends on the specimen size and is proportional to $\alpha\psi a^{1/2}$. As demonstrated in Fig. 3, for small specimens, K_Q and $\alpha\psi a^{1/2}$ obey a linear correlation with the fracture strength $\sigma_f = 2.8$ GPa obtained by linear fitting, consistent with the net-section fracture stress $\sigma_e = 2.9$ GPa calculated from experimental data [18].

To understand the transition from the fracture toughness-dominated fracture to fracture strength-dominated fracture as the specimen scales down, an approach is developed combining the Griffith strength theory and damage mechanics. According to the Griffith theory, the fracture strength σ_f of a brittle plate with a through microcrack of length $2a$ is [2,5]

$$\sigma_f = \sqrt{\frac{EG}{\pi a}}, \tag{5}$$

where E is Young's modulus and G is the fracture surface energy. σ_f can then be rewritten as

$$\sigma_f = \frac{K_Q}{\sqrt{\pi a}} \tag{6}$$

by introducing the equivalency between fracture toughness K_Q and fracture surface energy G as $G = K_Q^2/E$.

Based on the experimental results in Ref. [18], K_Q for the large specimen is around 3.2 MPa m$^{1/2}$ as the inherent fracture toughness of the model material, and the fracture strength σ_f is 2.8 GPa as derived from linear fitting. Thus, via Eq. (6), the length of the microcrack can be determined as 0.85 μm. From the viewpoint of elastic-damage law [30,31], initially the material deforms elastically, but the damage fracture suddenly occurs once the fracture strength is reached. Incorporating this law with the Griffith theory, the brittle fracture can be interpreted as follows. For a crack-free specimen subjected to the tensile loading, as the applied stress reaches the critical value (fracture strength σ_f), there comes rapid damage, and a damage zone appears without load-carrying capacity [see Fig. 4(a) for illustration]. Here we assume that the size of the damage zone is equal to that of the microcrack of the Griffith theory (0.85 μm). As a result, the Griffith fracture condition is satisfied and, simultaneously, catastrophic failure occurs. In other words, nucleating the damage zone corresponds identically with the catastrophic failure.

For the specimens with crack length of 0.2 μm–2.1 μm, before the stress intensity factor K approaches the critical value K_Q, the net-section stress reaches the fracture strength σ_f, and a damage zone rapidly appears with a length of around 0.85 μm. Therefore, the fracture of these specimens is controlled by the strength criterion. Because the ligaments of two smallest specimens in Ref. [18] are 0.6 μm and 1 μm long, respectively, less than or almost equal to the damage zone size, the two specimens fractured catastrophically within

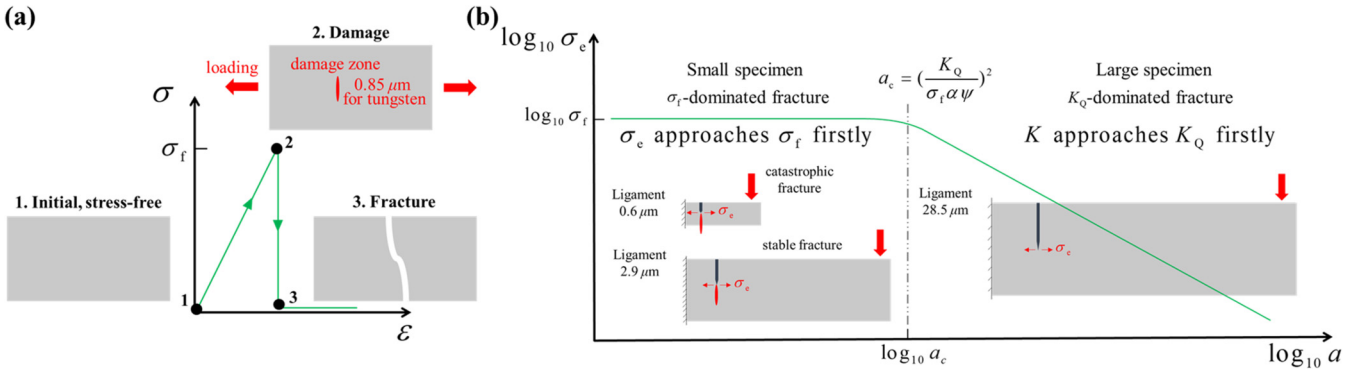

FIG. 4. Coupling the Griffith strength theory and elastic-damage law to illustrate the fracture behavior of brittle materials. (a) For a crack-free specimen under the tensile condition, as the loading stress increases to the fracture strength σ_f, a damage zone rapidly generates with a size equal to the Griffith flaw, and catastrophic fracture occurs. (b) For a microcantilever with a pre-existing crack, the fracture criterion is related to the crack length. For small specimens with $a < a_c$, the net-section stress σ_e reaches the critical value σ_f first, and the fracture is controlled by the strength. In the case of extremely small specimens, the ligament ahead of the crack is less than the damage zone size, and catastrophic fracture happens. For large specimens with $a > a_c$, the stress intensity factor K first reaches the critical value K_Q, and the fracture is controlled by the fracture toughness.

the nearly linear-elastic region [Fig. 4(b)]. For the specimens with ligaments 1.8 μm and 2.9 μm (significantly larger than the identified damage zone size 0.85 μm), the crack extends but does not cover the whole uncracked area [Fig. 4(b)]. This explains the phenomenon in Ref. [18] that the fracture of these two smallest specimens occurs almost within the elastic region while the larger ones exhibit stable fracture. For the specimens with ligaments of 9.5 μm and 28.5 μm, K first reaches the critical value K_Q, and the failure is controlled by the fracture toughness criterion.

As discussed above, the fracture of brittle materials is governed by the fracture strength or toughness, depending on which term first reaches the corresponding critical value. As indicated by the dashed line in Fig. 4(b), the critical crack length

$$a_c = \left(\frac{K_Q}{\sigma_f \alpha \psi}\right)^2 \tag{7}$$

deduced from Eq. (4) can be used to distinguish the fracture behavior. At $a < a_c$, the net-section stress first reaches σ_f, and the fracture is dominated by the strength. In this case, the fracture stress is independent of the crack length. At $a > a_c$, K reaches K_Q first, and the fracture is governed by the fracture toughness. In a log-log plot, the net-section fracture stress and the crack length exhibit a linear correlation.

In Fig. 5, we summarize the critical crack length a_c of brittle materials based on reported experimental data (see Part 4 in the SM for details [22]). Among these studies, only for silicon compounds, the crack length a is significantly larger than the critical crack length a_c (illustrated in Fig. 5) and the fracture toughness characterized at the microscale is in agreement with that at the macroscale [32]. For metallic glasses and intermetallics, a is several orders of magnitude smaller than a_c. The corresponding net-section fracture stress is close to or significantly larger than the fracture strength. This indicates that the fracture could be controlled by the fracture strength instead of the fracture toughness, and explains why the fracture toughness of Zr-based metallic glasses, NiAl and TiAl intermetallics measured at the macroscale is about 50 MPa m$^{1/2}$, 8 MPa m$^{1/2}$, and 20 MPa m$^{1/2}$, respectively, significantly larger than the microscale values of 5 MPa m$^{1/2}$, 5 MPa m$^{1/2}$, and 3.7 MPa m$^{1/2}$, respectively [9,33–39].

Our analysis also sheds light on the macroscale fracture of materials with high fracture toughness. For instance, it is reported that the measured fracture toughness of the precipitation hardening high strength steel is about 110 MPa m$^{1/2}$ when the specimen size satisfies the ASTM standard [40]. As the specimen size equally scales down, the fracture toughness measured decreases. Based on our model, we find that the crack length a of the small specimen is less than a_c (illustrated in Fig. 5), and the decrease of the fracture toughness with the specimen size is mainly due to the change of fracture mechanism (see Part 5 in the SM for detailed discussion [22]).

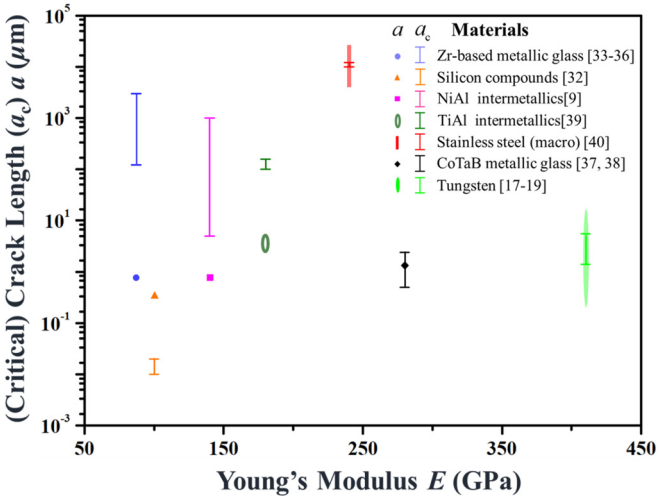

FIG. 5. Summary of crack length a (polygons) and critical crack length a_c (bars) in the mechanical fracture testing of different brittle materials.

III. SUMMARY

The present paper demonstrates that as the size of the brittle materials scales down to a critical value, the fracture toughness-controlled fracture changes to strength-controlled fracture. This indicates that the fracture behavior of the large specimen is dominated by the stress level around the crack tip, i.e., stress intensity factor, while for the small specimen it is determined by the stress level on the net section. The concept can be used to explain the phenomenon reported on the biocomposites whose mineral platelet is minimized to below a critical length so it is insensitive to cracklike flaw and possesses a high strength [41].

To appropriately characterize the fracture toughness, the crack length shall be sufficiently large not only to ensure the exact description of the stress field via LEFM, but also to guarantee that the net-section stress is considerably less than the fracture strength. Moreover, based on our model, the critical crack length a_c, regulating the fracture mechanisms, is proportional to the ratio between the fracture toughness and fracture strength. For the material of low fracture toughness and high strength, a_c is in a range from microscale down to nanoscale, while for the material of high toughness and high strength, a_c is on the order of millimeters.

ACKNOWLEDGMENTS

We thank Dr. Johannes Ast for providing the data of specimen size and the financial support by the National Natural Science Foundation of China under Grants No. 11632001, No. 11521202, and No. U1830121, the Science Challenge Project No. TZ2018001, and the ENN Science and Technology Development Co. Ltd. under Grant No. 9710L2018-001.

[1] A. P. Mouritz, *Introduction to Aerospace Materials* (Woodhead Publishing, Cambridge, UK, 2012), pp. 454–468.
[2] B. Lawn, *Fracture of Brittle Solids*, 2nd ed. (Cambridge University Press, New York, USA, 1993), pp. 1–40.
[3] C. K. H. Dharan, B. S. Kang, and I. Finnie, *Finnie's Notes on Fracture Mechanics: Fundamental and Practical Lessons* (Springer, New York, 2016), pp. 95–131.
[4] ASTM E399-17, Standard Test Method for Linear-Elastic Plane-Strain Fracture Toughness K_{Ic} of Metallic Materials, West Conshohocken, USA, 2017.
[5] Z. P. Bažant, J. Eng. Mech. **110**, 518 (1984).
[6] C. Yin, D. Terentyev, T. Pardoen, R. Petrov, and Z. Tong, Mater. Sci. Eng. A **750**, 20 (2019).
[7] S. S. Luo, Z. S. You, and L. Lu, Scr. Mater. **133**, 1 (2017).
[8] M. G. Mueller, V. Pejchal, G. Žagar, A. Singh, M. Cantoni, and A. Mortensen, Acta Mater. **86**, 385 (2015).
[9] F. Iqbal, J. Ast, M. Göken, and K. Durst, Acta Mater. **60**, 1193 (2012).
[10] Y. Xiang, X. Chen, and J. J. Vlassak, J. Mater. Res. **20**, 2360 (2011).
[11] G. Wu, K. C. Chan, L. Zhu, L. Sun, and J. Lu, Nature **545**, 80 (2017).
[12] C. Lee, X. D. Wei, J. W. Kysar, and J. Hone, Science **321**, 385 (2008).
[13] C. Motz, T. Schöberl, and R. Pippan, Acta Mater. **53**, 4269 (2005).
[14] O. Torrents Abad, J. M. Wheeler, J. Michler, A. S. Schneider, and E. Arzt, Acta Mater. **103**, 483 (2016).
[15] J. Ast, B. Merle, K. Durst, and M. Göken, J. Mater. Res. **31**, 3786 (2016).
[16] J. Weissmüller and H. L. Duan, Phys. Rev. Lett. **101**, 146102 (2008).
[17] C. Bohnert, N. J. Schmitt, S. M. Weygand, O. Kraft, and R. Schwaiger, Int. J. Plast. **81**, 1 (2016).
[18] J. Ast, M. Göken, and K. Durst, Acta Mater. **138**, 198 (2017).
[19] S. Wurster, C. Motz, and R. Pippan, Philos. Mag. **92**, 1803 (2012).
[20] G. Y. Jing, H. L. Duan, X. M. Sun, Z. S. Zhang, J. Xu, Y. D. Li, J. X. Wang, and D. P. Yu, Phys. Rev. B **73**, 235409 (2006).
[21] Y. Zou, P. Okle, H. Yu, T. Sumigawa, T. Kitamura, S. Maiti, W. Steurer, and R. Spolenak, Scr. Mater. **128**, 95 (2017).
[22] See Supplemental Material at http://link.aps.org/supplemental/10.1103/PhysRevMaterials.3.113602 for the introduction on fracture toughness testing at the macroscale and microscale, construction of the standard to specify the specimen size of the cantilever configuration, simulation results on bending stress, and applications of our model.
[23] L. Xiong, Z. S. You, S. D. Qu, and L. Lu, Acta Mater. **150**, 130 (2018).
[24] R. Pippan, S. Wurster, and D. Kiener, Mater. Des. **159**, 252 (2018).
[25] J. Riedle, P. Gumbsch, and H. F. Fischmeister, Phys. Rev. Lett. **76**, 3594 (1996).
[26] J. M. Liu and B. W. Shen, Metall. Mater. Trans. A **15**, 1289 (1984).
[27] E. I. Preiß, B. Merle, and M. Göken, Mater. Sci. Eng. A **691**, 218 (2017).
[28] J. Ast, T. Przybilla, V. Maier, K. Durst, and M. Göken, J. Mater. Res. **29**, 2129 (2014).
[29] W. F. Brown and J. E. Srawley, Plane strain toughness testing of high strength metallic materials, in *Plane Strain Crack Toughness Testing of High Strength Metallic Materials* (American Society for Testing and Materials, West Conshohocken, USA, 1966) pp. 16–25.
[30] H. D. Bui and A. Ehrlacher, Propagation of damage in elastic and plastic solids, in *Advances in Fracture Research*, edited by D. Francois *et al.* (Pergamon Press, Oxford, UK, 1981), Vol. 3, pp. 533–551.
[31] J. L. Chaboche, Nucl. Eng. Des. **105**, 19 (1987).
[32] K. Matoy, H. Schonherr, T. Detzel, T. Schoberl, R. Pippan, C. Motz, and G. Dehm, Thin Solid Films **518**, 247 (2009).
[33] V. Schnabel, B. N. Jaya, M. Kohler, D. Music, C. Kirchlechner, G. Dehm, D. Raabe, and J. M. Schneider, Sci. Rep. **6**, 36556 (2016).
[34] Y. Y. Cheng, S. Pang, C. Chen, and T. Zhang, J. Alloys Compd. **688**, 724 (2016).
[35] C. L. Li, J. P. Chu, and J. W. Lee, Mater. Sci. Eng. A **698**, 104 (2017).
[36] Z. Q. Liu and Z. F. Zhang, J. Appl. Phys. **115**, 163505 (2014).

[37] P. Kontis, M. Kohler, S. Evertz, Y. T. Chen, V. Schnabel, R. Soler, J. Bednarick, C. Kirchlechner, G. Dehm, D. Raabe *et al.*, Scr. Mater. **155**, 73 (2018).

[38] J. Li, Y. W. Wang, J. Yi, I. Hussain, R. Li, B. Zhang, and G. Wang, J. Alloys Compd. **680**, 43 (2016).

[39] T. P. Halford, K. Takashima, Y. Higo, and P. Bowen, Fatigue Fract. Eng. Mater. Struct. **28**, 695 (2005).

[40] Q. Q. Duan, B. Wang, P. Zhang, R. T. Qu, and Z. F. Zhang, Chin. J. Mater. Res. **32**, 561 (2018).

[41] H. Gao, B. Ji, I. L. Jäger, E. Arzt, and P. Fratzl, Proc. Natl. Acad. Sci. **100**, 5597 (2003).